crystals

MDPI

Article

# Synthesis of Enaminones-Based Benzo[*d*]imidazole Scaffold: Characterization and Molecular Insight Structure

**Saeed Alshahrani [1], Saied M. Soliman [2], Abdullah Saleh Alamary [1], Abdullah Mohammed Al-Majid [1,*], Matti Haukka [3], Sammer Yousuf [4] and Assem Barakat [1,2,*]**

1 Department of Chemistry, College of Science, King Saud University, P.O. Box 2455, Riyadh 11451, Saudi Arabia; chemistry99y@gmail.com (S.A.); alamary1401@yahoo.com (A.S.A.)
2 Department of Chemistry, Faculty of Science, Alexandria University, P.O. Box 426, Ibrahimia, Alexandria 21321, Egypt; saied1soliman@yahoo.com
3 Department of Chemistry, University of Jyväskylä, P.O. Box 35, FI-40014 Jyväskylä, Finland; matti.o.haukka@jyu.fi
4 H.E.J. Research Institute of Chemistry, International Center for Chemical and Biological Sciences, University of Karachi, Karachi-75270, Pakistan; dr.sammer.yousuf@gmail.com
* Correspondence: amajid@ksu.edu.sa (A.M.A.-M.); ambarakat@ksu.edu.sa (A.B.); Tel.: +966-11467-5901 (A.B.); Fax: +966-11467-5992 (A.B.)

Received: 16 September 2020; Accepted: 18 October 2020; Published: 21 October 2020


**Abstract:** (*E*)-1-(1*H*-Benzo[*d*]imidazol-2-yl)-3-(dimethylamino)prop-2-en-1-one **2** was synthesized by one-pot synthesis protocol of 2-acetyl benzo[*d*]imidazole with dimethylformamide dimethylacetal (DMF-DMA) in xylene at 140 °C for 8 h. Reaction of enaminone derivative **1** with acetylacetone in the presence of AcOH/$NH_4OAc$ under reflux afforded the cyclized pyridino-benzo[*d*]imidazole derivative **3**. The latter compound was converted into the corresponding *β*-enaminone **4** with DMF-DMA. The single crystal X-ray diffraction technique eventually confirmed the assigned chemical structure of the *N*-alkyl-*β*-enaminone **2** and pyridino-benzo[*d*]imidazole derivative **3**. *N*-alkyl-*β*-enaminone **2** crystallized in the monoclinic space group $P2_1/n$ with unit cell parameters of **a** = 9.8953(3) Å, **b** = 5.7545(2) Å, **c** = 21.7891(7) Å, and β =100.627(2)°, and with one molecule per asymmetric unit. On the other hand, compound **3** crystallized in the orthorhombic crystal system and space group $P2_12_12_1$ with unit cell parameters of **a** = 6.82950(10) Å, **b** = 8.00540(10) Å, **c** = 22.4779(2) Å, and also with one molecule per asymmetric unit. Based on Hirshfeld analysis, the H...H (51.3%), O...H (10.0%), N...H (10.3%), and C...H (27.6%) contacts in **2** and the H...H (46.8%), O...H (9.9%), N...H (13.0%), and C...H (21.6%) in addition to the C . . . C (6.7%) interactions in **3** are the most important towards crystal stability via molecular packing. The main difference is the presence of π–π interaction among the molecular units of **3** but not in **2**. The calculated $^1$H and $^{13}$C NMR chemical shifts showed good agreements with experimental data. Electronic properties and reactivity parameters of both compounds are also calculated and compared.

**Keywords:** benzo[*d*]imidazole; *β*-enaminone; DMF-DMA; Hirshfeld analysis; DFT

## 1. Introduction

Fused heterocycles based on benzimidazoles scaffold have been found in many biologically active natural products and pharmaceutical drugs [1]. This extraordinary benzimidazole privileged structure showed pharmacological features like antiviral [2–4], antimicrobial [5], antioxidant [6], antidiabetic [7], antihelmintics [8], antiparasitic [9], antiproliferative [6], anticancer activity [10,11],

anti-inflammatory [12], anticonvulsant, central nervous system (CNS) depressant, proton pump inhibitor, antihypertensive, antineoplastic, and antitrichinellosis [13].

Polydentate enaminone reagents have gained more attention in the last decade due to their utilization as synthons in organic synthesis transformation [14–16]. These building blocks have dual electronic attitude and can be employed as electrophilic enones or act as nucleophilic enones in many chemical transformations for the construction of many cyclic compounds with interesting biological activities as antibacterial, antitumor, anti-convulsant, and anti-glycating agents, as well as enzyme inhibitors [17–22]. The structural features of the pharmacophore play a crucial role for the biological activity of the compound. Combining two pharmacophores in one hybrid is a challenge.

Pyridine scaffold is a very important skeleton of the heterocyclic family which exists as core structure in many divergent natural products such as alkaloids, coenzymes, and vitamins. Furthermore, it is used in a large scale in industrial chemistry for the synthesis of many products such as herbicide, bactericide, and insecticide. Additionally, in biological sciences, it has been approved to have a high pharmacological importance [23,24].

In this text and the continuation of our research program towards the synthesis of new heterocyclic hybrids [25–30], we explored the synthesis of two $\beta$-enaminones based on benzo[*d*]imidazole scaffolds by mixing 2-acetyl benzo[*d*]imidazole with dimethylformamide dimethylacetal (DMF-DMA) in xylene under thermal conditions.

The molecular structure of the synthesized $\beta$-enaminones was elucidated by spectrophotometric tools including NMR spectra. The structural features of $\beta$-enaminone **2** and **3** were assigned eventually by X-ray single crystal analysis combined with density functional theory (DFT) calculations and Hirshfeld analysis.

## 2. Materials and Methods

General:

The $^{1}$H-and $^{13}$C-NMR spectra of both $\beta$-enaminones were recorded on a JEOL 400MHz spectrometer (JEOL, Ltd., Tokyo, Japan) at ambient temperature. The solvent used was DMSO-$d_6$; the chemical shifts ($\delta$) are given in ppm. The topology analyses were performed using the Crystal Explorer 17.5 program [31]. All DFT calculations were performed using the Gaussian 09 software package [32,33] utilizing the B3LYP/6-31G(d,p) method. Natural population analysis was performed using the NBO 3.1 program as implemented in the Gaussian 09W package [34]. The self-consistent reaction filed (SCRF) method [35,36] was used to model the solvent effects when calculating the optimized geometries in solution. Then, the NMR chemical shifts for the protons and carbons were computed using the GIAO method in the same solvent (DMSO) [37].

### *2.1. (E)-1-(1H-Benzo[d]imidazol-2-yl)-3-(dimethylamino)prop-2-en-1-one* ***1***

The reaction mixture of 2-acetyl benzimidazole (1.60 g, 10 mmol) and DMF-DMA (1.19 g, 10 mmol) in xylene (40 mL) was refluxed for 3 h, then the reaction mixture was allowed to cool at room temperature. The precipitated solid product was isolated by simple filtration and subsequently washed with petroleum ether to afford compound **2** in a pure form as yellowish brown crystals.

Yield (1.98 g, 92%), mp 226–228 °C. $^{1}$H NMR (400 MHz, DMSO-$d_6$) $\delta$: 2.9 6(s, 3H, $CH_3$), 3.2(s, 3H, $CH_3$), 6.26 (d, 1H, CH, $J$ = 7.2 Hz), 7.13–7.26 (m, 2H, imidazole-H), 7.61 (brs, 2H, imidazole-H), 7.88(d, 1H, CH, $J$ = 7.2 Hz), 12.95(s, 1H, NH); $^{13}$C NMR (100MHz, DMSO-$d_6$): 177.96(C O), 154.62 (=**C**N), 151.76,(122.85, 123.11, aromatic carbons), 91.16 (=**C**), 45.28 (N**C**$H_3$), 37.81 (N**C**$H_3$); [Anal. Calcd. for $C_{12}H_{13}N_3O$; Calcd.: C, 66.96; H, 6.09; N, 19.52; Found: C, 67.01; H, 6.00; N, 19.42].

### *2.2. (E)-3-(Dimethylamino)-1-(1-methyl-1H-benzo[d]imidazol-2-yl)prop-2-en-1-one* **2**

The reaction mixture of 2-acetyl benzimidazole (1.60 g, 10 mmol) and DMF-DMA (1.55 g, 13 mmol) in xylene (40 mL) was refluxed at 140 °C for 8 h. The reaction mixture was cooled down to room temperature and left for a period of time to give product **2** in a pure form as yellowish brown crystals.

Yield 71%, mp 228–230 °C. $^1$H NMR (400 MHz, DMSO-$d_6$) δ: 2.93 (s, 3H, $CH_3$), 3.18 (s, 3H, $CH_3$), 4.11 (s, 3H, N**C**$H_3$), 6.27 (d, 1H, CH, *J* = 12.4 Hz), 7.28 (t, 1H, *J* = 8.0Hz, imidazole-H), 7.34 (t, 1H, *J* = 8.0 Hz, imidazole-H), 7.59 (d, 1H, *J* = 8.0 Hz, imidazole-H), 7.75 (d, 1H, *J* = 8.0 Hz, imidazole-H), 7.83 (d, 1H, CH, *J* = 12.4 Hz); $^{13}$C NMR (100 MHz, DMSO-$d_6$): 179.85 (**C**O), 154.49 (=**C**N), 149.53, 141.76, 137.22, 124.42, 123.16, 120.93, 120.57, 111.51, 93.69 (=**C**), 45.22 (N**C**$H_3$), 37.77 (N**C**$H_3$), 32.53 (N-$CH_3$); Figures S1 and S2 (Supplementary Materials). [Anal. Calcd. for $C_{13}H_{15}N_3O$; Calcd.: C, 68.10; H, 6.59; N, 18.33; Found: C, 68.29; H, 6.62; N, 18.10].

### *2.3. 1-(6-(1H-Benzo[d]imidazol-2-yl)-2-methylpyridin-3-yl)ethan-1-one* **3**

A mixture of **1** (0.432 g, 2 mmol), acetylacetone (0.20 g, 2 mmol), and ammonium acetate (0.385 g, 5 mmol) in 15 mL of acetic acid was refluxed for 4–6 h. The progress of the reaction was monitored by using thin layer chromatography (TLC). After completion, 50 mL ice-cold water was added to the reaction mixture and neutralized with a solution of $NaHCO_3$ leading to a pale brown precipitate of **3** which was filtered and dried.

Pale brown solid; yield (84%); mp: 191–193 °C; $^1$H NMR (DMSO–$d_6$, 400 MHz): δ 13.01 (1H, s, NH), 8.37 (1H, d, *J* = 8 Hz, Py-H), 8.25 (1H, d, *J* = 8 Hz, Py-H), 7.65 (2H, m, ArH), 7.24 (2H, m, ArH), 2.75 (3H, s, $CH_3$), 2.60 (3H, s, $COCH_3$); $^{13}$C NMR (DMSO–$d_6$, 100 MHz): δ = 200.28, 157.32, 149.84, 149.23, 143.95, 138.68, 132.48, 123.38, 122.66, 119.33, 118.64, 112.33, 29.38, 24.46; Figures S3 and S4 (Supplementary Materials). [Anal. Calcd. for $C_{15}H_{13}N_3O$; Calcd.: C, 71.70; H, 5.21; N, 16.72; Found: C, 71.68; H, 5.25; N, 16.70].

### *2.4. (E)-1-(6-(1H-benzo[d]imidazol-2-yl)-2-methylpyridin-3-yl)-3-(dimethylamino)prop-2-en-1-one* **4**

To 1-(6-(1*H*-benzo[d]imidazol-2-yl)-2-methylpyridin-3-yl)ethanone (0.251 g, 1 mmol) in xylene (20 mL) was added dimethylformamide dimethylacetal DMF-DMA (1.31 g, 1.1 mmol). The reaction was refluxed for 8 h, then allowed to cool. The resulting solid was filtered to afford the pure product.

White solid; yield (78%); mp: 225–227 °C; $^1$H NMR (DMSO–$d_6$, 400 MHz): δ 12.87 (1H, s, NH), 8.12 (1H, d, *J* = 8 Hz, =CH), 7.80 (1H, m, ArH), 7.66 (1H, d, *J* = 7.5 Hz, Py-H), 7.55 (1H, d, *J* = 7.5 Hz, Py-H), 7.21–7.17 (3H, m, ArH), 5.34 (1H, d, *J* = 8 Hz, =CH), 3.06 (3H, s, $NCH_3$), 2.83 (3H, s, $NCH_3$), 2.57 (3H, s, $CH_3$); $^{13}$C NMR (DMSO–$d_6$, 100 MHz): δ = 155.75, 150.99, 147.82, 144.35, 136.48, 135.38, 123.70, 122.50, 119.74, 119.01, 112.72, 45.07, 37.60, 23.41; Figures S5 and S6 (Supplementary Materials). [Anal. Calcd. for $C_{18}H_{18}N_4O$; Calcd.: C, 70.57; H, 5.92; N, 18.29; Found: C, 70.64; H, 5.88; N, 18.34].

## 3. Results and Discussion

### *3.1. Synthesis of β-enaminones*

The synthesis of *β*-enaminones-based benzo[*d*]imidazole **1** and **2** have been reported before [38–42], but a direct method to reach the final *β*-enaminone **2** from the starting material 2-acetyl benzo[*d*]imidazole has not been reported to the best of our knowledge. The synthesis of *N*-alkyl-*β*-enaminone-based benzo[*d*]imidazole scaffold **2** was achieved by a reaction of 2-acetyl benzo[*d*]imidazole with DMF-DMA as outlined in Scheme 1. The formation of compound **1** was obtained at 125 °C but was unprecedented. The *N*-methyl-*β*-enaminone **2** was obtained by restarting the reaction at higher temperature of 140 °C. The plausible mechanism for *N*-alkylation transformation of **1** to **2** via deprotonation of the NH of the imidazole ring to generate the more powerful nuclophile subsequently attack the electrophilic center of the (methoxymethylene)dimethyl-azonium ion to form the final compound **2**. The chemical structure of the *N*-alkyl-*β*-enaminone-based benzo[*d*]imidazole scaffold **2,** eventually confirmed by X-ray single crystal analysis, is consistent with the one reported before [38–42].

Further, the *β*-enaminones-based benzo[*d*]imidazole **1** was cyclized with the acetylacetone, and ammonium acetate in acetic acid, and refluxed for 4–6 h to afford the substituted pyridine-*β*-enaminones-based benzo[*d*]imidazole **3**. Luckily, suitable single crystals were obtained for compounds **2** and **3,** which support the $^{1}$H and $^{13}$C-NMR spectral analyses, and confirmed the chemical features of these compounds. Finally, compound **3** was converted into substituted pyridine-*β*-enaminones-based benzo[*d*]imidazole **4**.

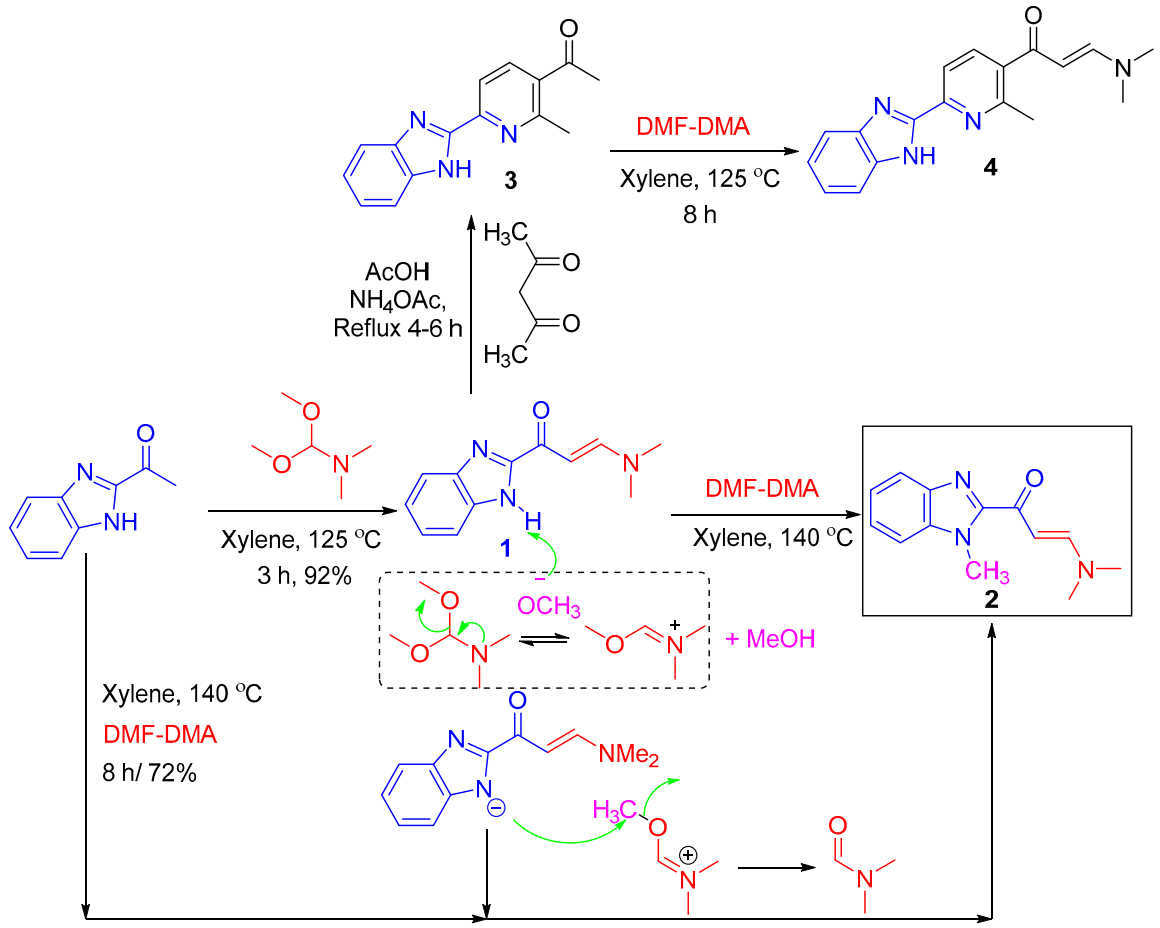


**Scheme 1.** Synthesis of *β*-enaminone based benzo[*d*]imidazole scaffolds **1**, **2** and **4**.

### *3.2. X-ray Structure*

The *β*-enaminone 2 crystallized in the monoclinic space group $P2_1/n$ with $Z = 4$ (Table 1). A list of bond distances and angles are provided in Table S1 (Supplementary Materials). The asymmetric unit comprised one perfectly planar molecule (Figure 1, upper part). Even the side chain and the benzo[*d*]imidazole moiety are also coplanar with a maximum deviation of 0.335 Å of C13 from the benzo[*d*]imidazole mean plane. The molecules are connected to form a three-dimensional network by C-H ... O and C-H ... $\pi$ interactions shown in Figure 2 (upper left part). Each two molecules are interconnected by C12-H12 ... O1 with a donor–acceptor distance of 3.347(3) Å, then the resulting dimeric units are further connected by weak C-H ... $\pi$ interactions leading to the three-dimensional packing structure shown in Figure 2 (lower left part).

The structure of 3 crystallized in the orthorhombic crystal system and space group $P2_12_12_1$ with $Z = 4$ (Table 1). List of bond distances and angles are provided in Table S2 (Supplementary Materials). The asymmetric unit comprised one almost perfectly planar molecule (Figure 1, lower part). The phenyl and the benzo[*d*]imidazole moieties are deviated only by 4.23°. The molecules are connected by strong N-H ... O hydrogen bonds and weak C-H ... O interactions shown in Figure 2 (right part).

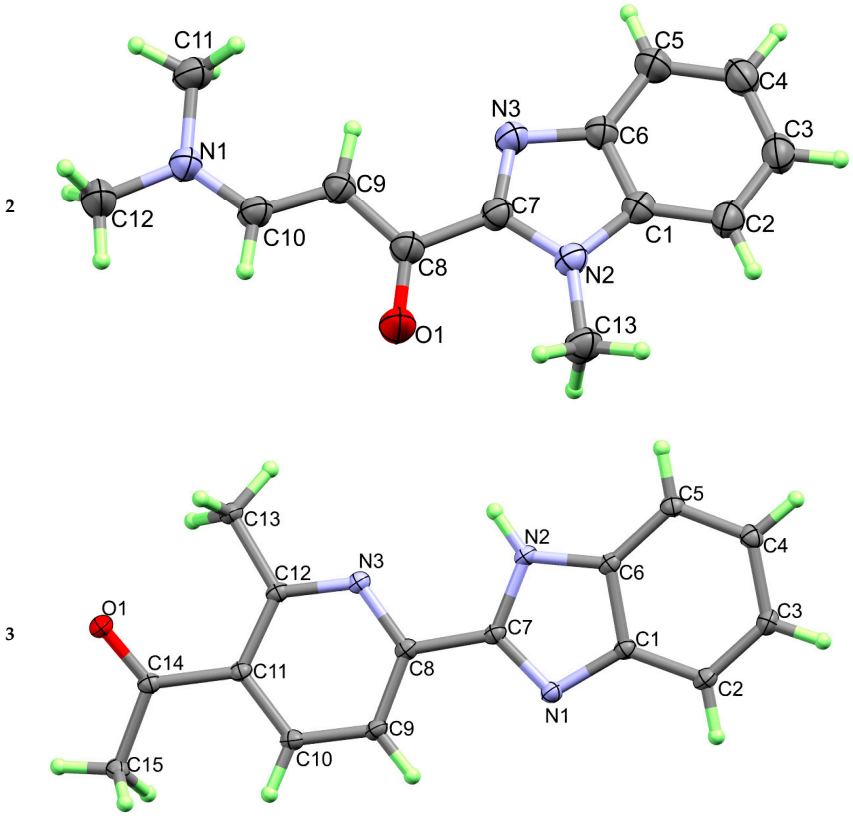


**Figure 1.** X-ray structure of **2** and **3**. Thermal ellipsoids were plotted at a 30% probability level.

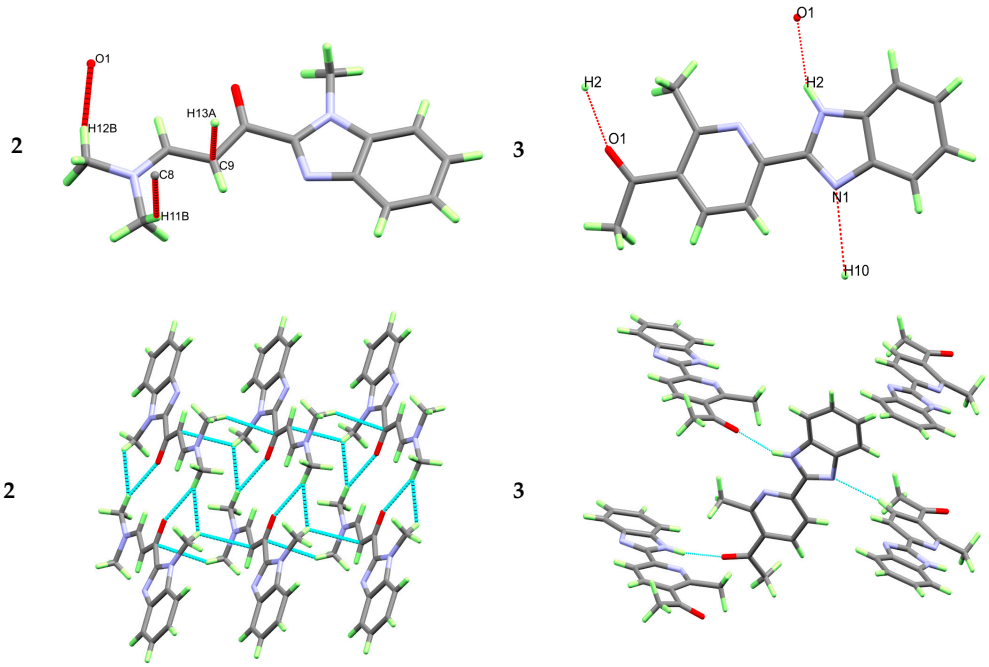


**Figure 2.** Intermolecular contacts (upper/left) and molecular packing (lower/left) of **2**. H-bond: C12-H12B: 0.98 Å, H12B···O1$^{\#1}$: 2.39 Å, C12···O1$^{\#1}$: 3.347(3) Å, C12-H12B···O1$^{\#1}$: 164.4° (equivalent position #1: 2-x,1-y,1-z). The C-H … π: C9 … H13A$^{\#2}$ (2.869 Å) and C8 … H11B$^{\#2}$ (2.816 Å), (equivalent position #2: x,1+y,z). Intermolecular contacts (upper/right) and molecular packing (lower/right) of **3**. C10-H10: 0.95 Å, H10···N1$^{\#1}$: 2.725 Å, C10···N1$^{\#1}$: 3.370(2) Å, C10-H10···N1$^{\#1}$: 125.78 (equivalent position #1: -1/2+x,1.5-y,1-z). N2-H2: 0.88 Å, H2···O1$^{\#2}$: 2.10 Å, N2···O1$^{\#2}$: 2.916(2) Å, N2-H2···O1$^{\#2}$: 153.9(2)° (equivalent position # 1-x,-1/2+y,1.5-z).

**Table 1.** Single crystal data and structure refinement details.

| **Compound** | **2** | **3** |
|---|---|---|
| CCDC code | 1999582 | 2032100 |
| Empirical formula | $C_{13}H_{15}N_3O$ | $C_{15}H_{13}N_3O$ |
| Formula weight | 229.28 | 251.28 |
| Temperature/K | 104(2) | 120(2) |
| Radiation | CuKα (λ = 1.54178) | CuKα (λ = 1.54178) |
| Crystal system | monoclinic | Orthorhombic |
| Space group | $P2_1/n$ | $P2_12_12_1$ |
| a/Å | 9.8953(3) | 6.82950(10) |
| b/Å | 5.7545(2) | 8.00540(10) |
| c/Å | 21.7891(7) | 22.4779(2) |
| β/° | 100.627(2) | |
| Volume/$Å^3$ | 1219.45(7) | 1228.93(3) |
| Z | 4 | 4 |
| Crystal size/$mm^3$ | 0.170 × 0.140 × 0.080 | 0.271 × 0.203 × 0.089 |
| $\rho_{calc}g/cm^3$ | 1.249 | 1.358 |
| $\mu/mm^{-1}$ | 0.657 | 0.710 |
| F(000) | 488 | 528 |
| 2Θ range for data collection/° | 4.13 to 68.20 | 3.933 to 77.074. |
| Index ranges | $-11 \le h \le 11, -6 \le k \le 6, -25 \le l \le 26$ | $-8 \le h \le 8, -10 \le k \le 10, -28 \le l \le 28$ |
| Reflections collected | 8164 | 29119 |
| Goodness-of-fit on $F^2$ | 1.057 | 1.072 |
| Data/restraints/parameters | 2209/0/157 | 2597/0/178 |
| Independent reflections | 2209 [$R_{int}$ = 0.0334] | 2597 [$R_{int}$ = 0.0313] |
| Final R indexes [all data] | $R_1$ = 0.0555, $wR_2$ = 0.1352 | $R_1$ = 0.0283, $wR_2$ = 0.0742 |
| Final R indexes [I ≥ 2σ (I)] | $R_1$ = 0.0464, $wR_2$ = 0.1268 | $R_1$ = 0.0288, $wR_2$ = 0.0747 |
| Largest diff. peak/hole/e $Å^{-3}$ | 0.18/–0.20 | 0.137/–0.217 |

### *3.3. Hirshfeld Analysis*

All Hirshfeld surfaces are given in Figures S7 and S8 (Supplementary Materials) while the percentages of the important contacts in compound 2 are depicted in Figure 3. It shows the possible contacts among molecular units and their percentage contributions. The H...H (51.3%), O...H (10.0%), N...H (10.3%), and C...H (27.6%) are the most important. As shown in Figure 4, the O...H contacts appeared as sharp red spots in the $d_{norm}$ with intense spikes in the fingerprint plot indicating significant and short contacts corresponding to the O1...H12B (2.294 Å) and O1...H10 (2.625 Å). The C...H contacts manifested as fad red spots in the $d_{norm}$ and relatively less intense spikes in the fingerprint, indicating relatively weak interactions with a C8...H11B distance of 2.728 Å. The N...H contacts appeared as white regions in the $d_{norm}$ map and broad spikes in the fingerprint plot with a relatively longer N3...H11A distance (2.692 Å) compared to the vdW radii sum of N and H atoms (2.64 Å). The common H...H interactions are found as blue regions in the $d_{norm}$ which reveal very weak interactions. It is worth to note that the Hirshfeld calculations of the almost similar published structure (CCDC code: LILJEW; 297714) [40] returned with almost similar results with slight variations in the interaction distances as shown in Figures S9–S11 (Supplementary Materials). In addition, the powder diffraction patterns of both crystals are almost identical (Figure S12).

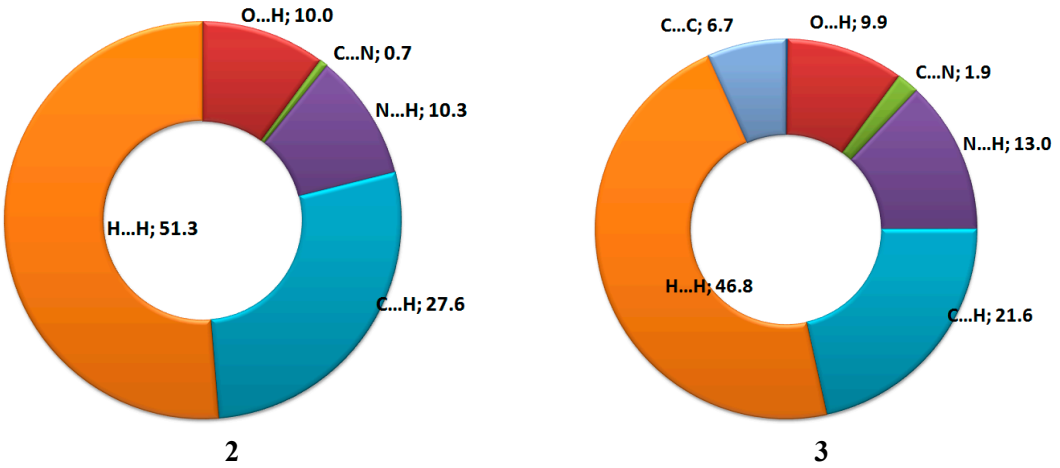


**Figure 3.** Different contacts and their percentage contributions in the studied compounds.

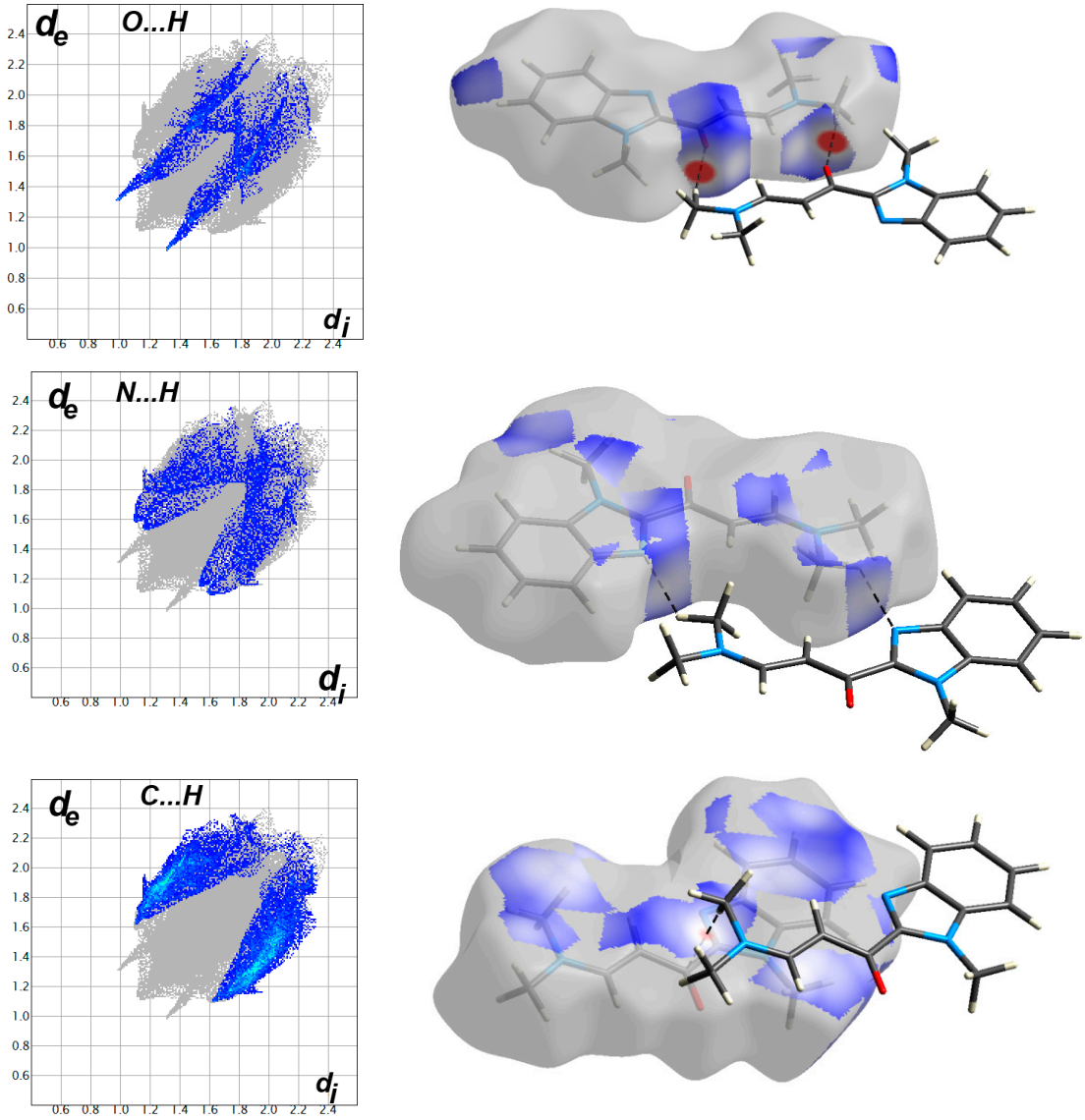


**Figure 4.** The O . . . H, C . . . H and N . . . H interactions in **2** observed using Hirshfeld analysis.

On the other hand, compound **3** crystal packing depends on a large contribution of H...H (46.8%), O...H (9.9%), N...H (13.0%), and C...H (21.6%) in addition to the C . . . C (6.7%) interactions (Figure 3). Similar to compound **2**, the O . . . H contacts are significant with the shortest O . . . H distance of 1.985 Å (O1 . . . H2) and the C . . . H interactions as well (Figure 5). The C7 . . . H15B (2.698 Å) and C2 . . . H3 (2.577) are the shortest C . . . H interactions. The major difference between the two compounds is the presence of π–π interaction among the molecular units of **3**. The shortest C . . . C distance is C4 . . . C8 (3.410 Å).

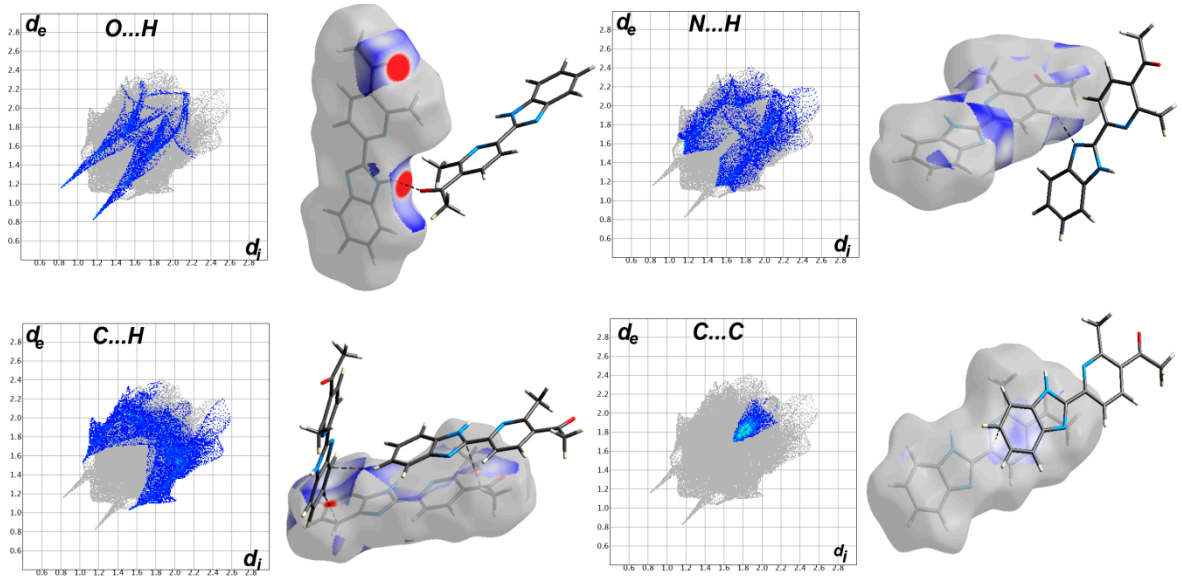


**Figure 5.** The O . . . H, C . . . H, C . . . C, and N . . . H interactions in **3** observed using Hirshfeld analysis.

### *3.4. DFT Studies*

The calculated geometries of the studied compounds match the experimental structures very well (Figure 6). Furthermore, the calculated bond distances and angles (Tables S3 and S4) correlated very well with the corresponding geometric parameters obtained from the X-ray structure with correlation coefficients of 0.9696–0.9951 and 0.9866–0.9931, respectively (Figure 7). The distribution of the natural charges and the molecular electrostatic potential mapped over electron density are shown in Figure 8. It is clear that the carbonyl oxygen and carbon atoms have the highest negative and positive charge in both molecules, respectively. As a result of this charge distribution, the calculated dipole moment values are 3.1956 and 0.3833 Debye for 2 and 3, respectively. It is possible to suggest that the low dipole moment of **3** could be attributed to the presence of almost similar electronegative atoms at both sides of the molecule connected by the C-C bond. Such an almost symmetrical situation could be a main reason for the low polarity of **3**. The direction of the dipole moment vector is from the dimethylamine group towards the imidazole moiety in **2** while it is almost passing through at the middle of the C-C bond in **3**.

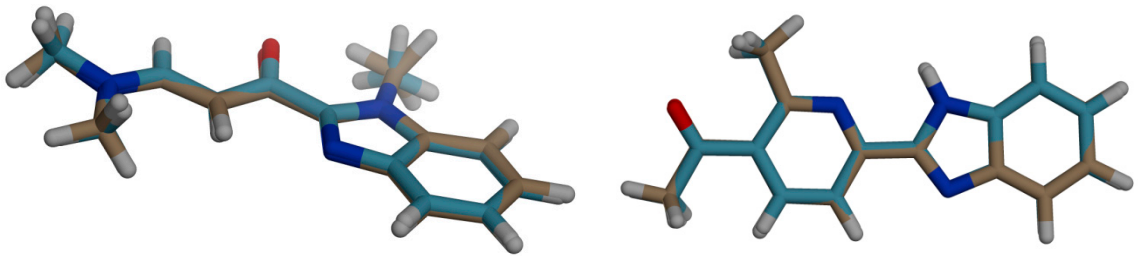


**Figure 6.** Overlay of the optimized and calculated structures for the studied organic compounds.

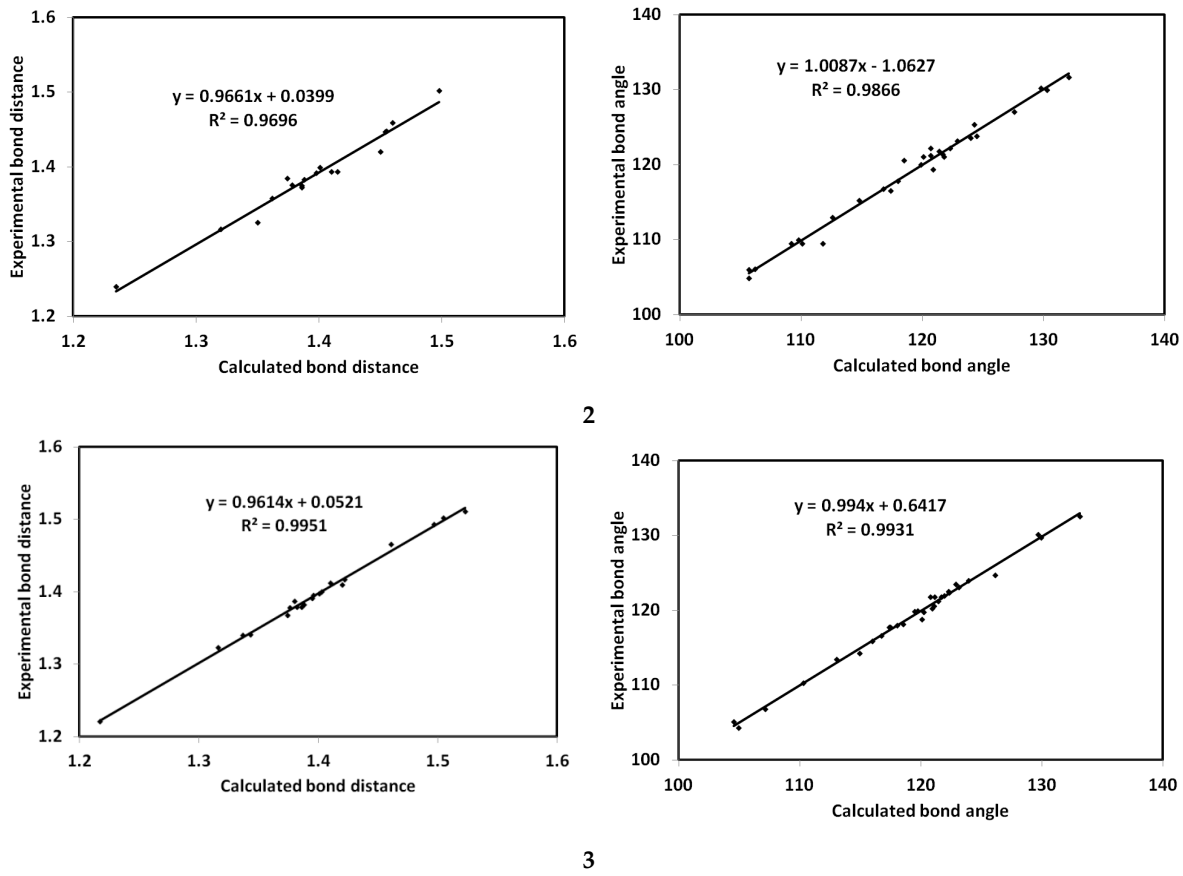


**Figure 7.** Correlation graphs (experimental and calculated) of *N*-methyl-*β*-enaminones (bond distance and angles).

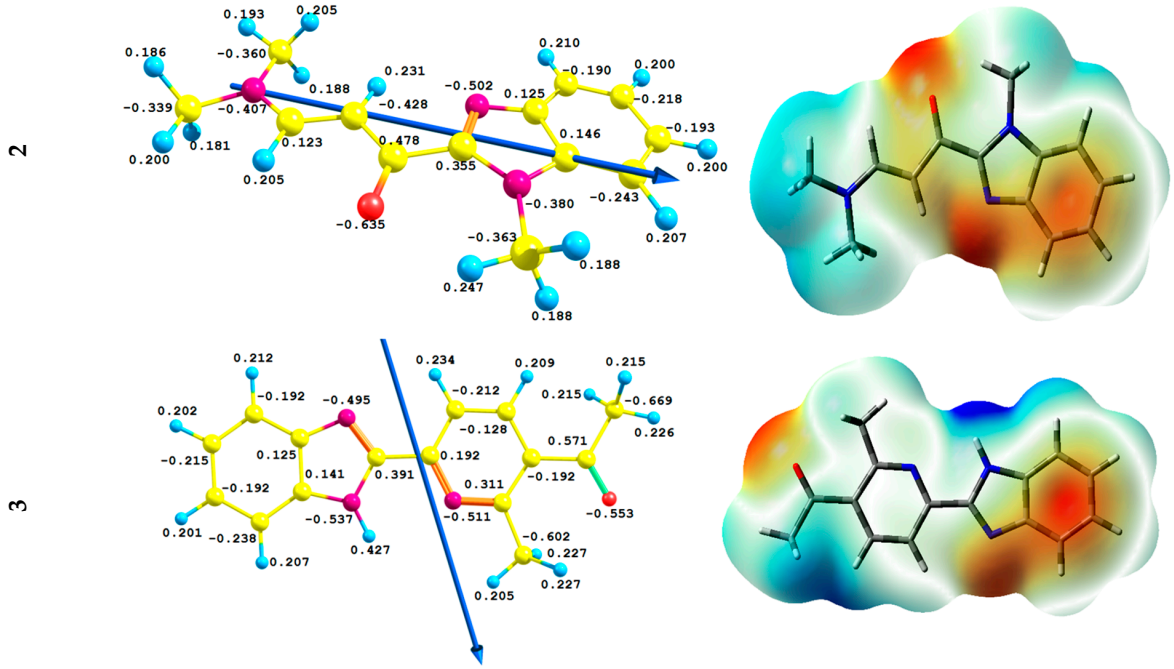


**Figure 8.** The natural charges over the optimized structure with dipole moment vector (**left**) and molecular electrostatic potential (MEP) map (**right**).

### *3.5. Reactivity Studies*

The reactivity indices based on the frontier molecular orbital energies for the studied compounds are calculated and compared [43–49]. The highest occupied (HOMO) and lowest unoccupied molecular orbital (LUMO) energies are calculated to be −5.7022 and −1.6409 eV, respectively, for **2**, while they are generally lower (−6.2162 and −2.4090 eV, respectively) in **3**. The reason could be related to the presence of a more conjugated system in **3** compared to **2**. As a result, electron affinity (A) and ionization potential (I) are 1.6409 and 5.7022 eV, respectively. The hardness (η = 4.0613), electrophilicity index (ω = 1.6596 eV), and chemical potential (μ = –3.6715 eV) were also computed using the frontier molecular orbitals energies. On the other hand, the corresponding values in **3** are 2.4090, 6.2162, 3.8072, 2.4426, and –4.3126 eV, respectively. It is clear that the intramolecular charge transfer represented by HOMO → LUMO excitation is easier in **3** than **2**. It is clear that both MOs are delocalized over the π-system indicating π–π* charge transfer-based transition (Figure 9). Moreover, compound **3** has a higher electrophilicity index indicating a higher ability to gain electron than **2** which agree very well with the low energy of LUMO in the former compared to the latter. In contrast, **2** is a better electron donor than **3**. The presented descriptors have a strong relation to the chemical reactivity of compounds.

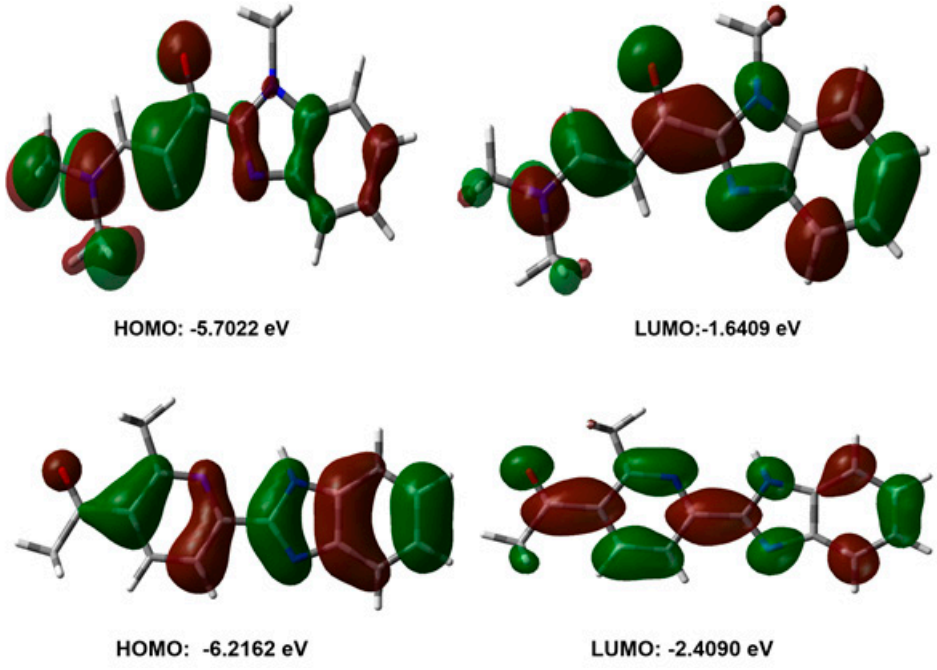


**Figure 9.** HOMO and LUMO orbital density of the *N*-methyl-*β*-enaminone **2** (**upper**) and compound **3** (**down**).

### *3.6. NMR Spectra*

The chemical shifts (C.S) of $^{1}$H and $^{13}$C were computed and the results are summarized in Tables S5–S6 (SI) in comparison with the results obtained experimentally. It is clear from Figure 10 that there is good correlation between the calculated and experimental C.S values. The correlation coefficients are 0.9818 for $^{1}$H-NMR and 0.9906 for $^{13}$C-NNMR in **2**. Similarly, for **3**, the correlation coefficients are 0.9372 and 0.9938, respectively.

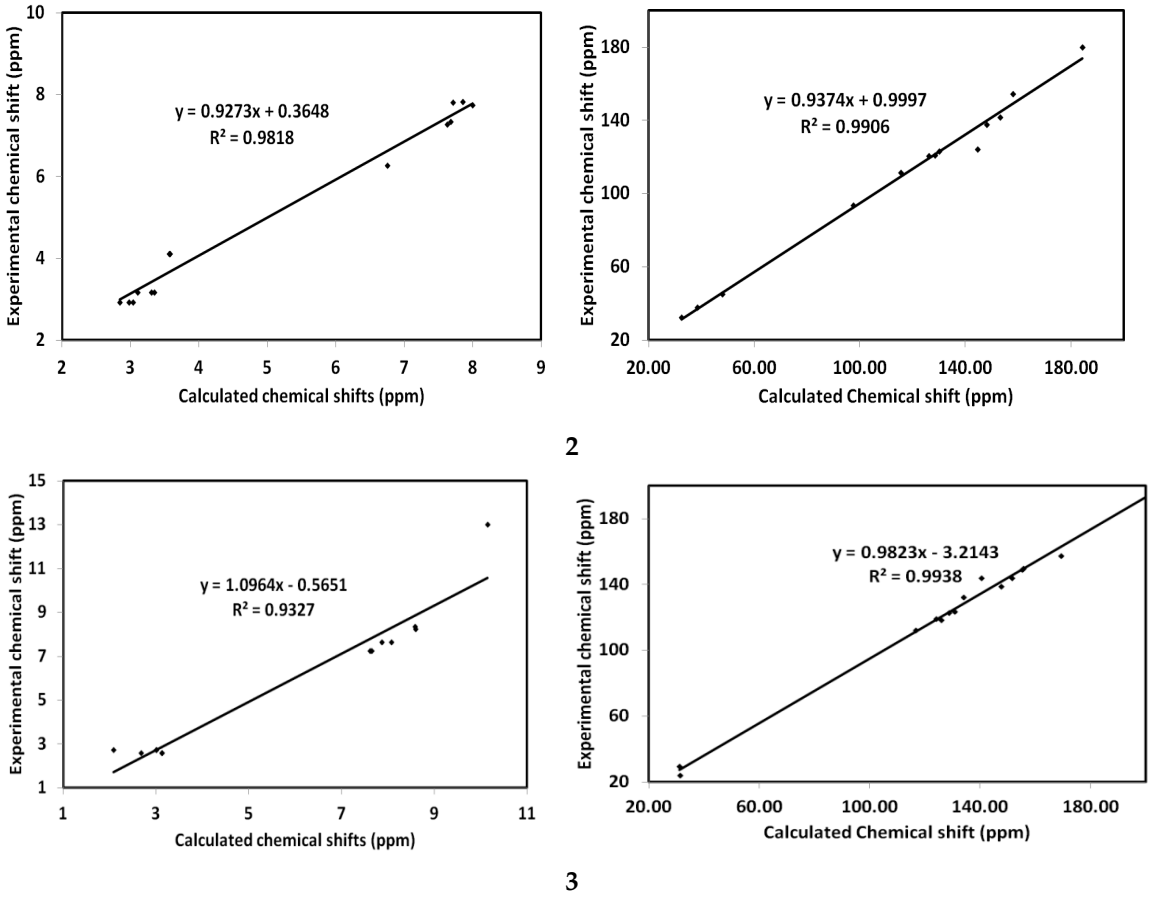


**Figure 10.** $^{1}$H and $^{13}$C NMR chemical shifts correlations.

## 4. Conclusions

The *N*-alkyl-*β*-enaminone-based benzo[*d*]imidazole scaffold **2** was obtained with a 72% yield at higher temperature (140 °C), but with a lower temperature of 125 °C, the reaction afforded **1**. Further, the cyclized pyridine-based benzo[*d*]imidazole and the corresponding *β*-enaminone were successfully achieved. The supramolecular structures of **2** and **3** were analyzed using Hirshfeld calculations. DFT calculations were used to compute the electronic properties of both systems. Some reactivity descriptors were also calculated based on the energies of the frontier molecular orbitals and then compared. Moreover, calculated NMR spectra are in good agreement with the experimental data.

**Supplementary Materials:** The following are available online at http://www.mdpi.com/2073-4352/10/10/955/s1, Figure S1: $^{1}$HNMR of 2; Figure S2: $^{13}$C-NMR of **2**; Figure S3: $^{1}$H-NMR of **3**; Figure S4: $^{13}$C-NMR of **3**; Figure S5: $^{1}$H-NMR of 4; Figure S6: $^{13}$C-NMR of 4, Figure S7: Hirshfeld surfaces of **2;** Figure S8: Hirshfeld surfaces of **3**; Figure S9: Hirshfeld surfaces of the previously published **2** (CCDC code: LILJEW; 297714); Figure S10: Different contacts and their percentage contributions in the previously published **2** (CCDC code: LILJEW; 297714); Figure S11: The O . . . H, C . . . H and N . . . H interactions in the previously published **2** (CCDC code: LILJEW; 297714); Figure S12: Powder X-ray diffraction patterns for the **2** (upper) and previously reported (CCDC code: LILJEW; 297714) lower; Figure S13: Atom numbering of the optimized structures of **2** (upper) and 3(lower) For details about DFT results; Table S1: Bond Lengths and Bond Angles for **2**; Table S2: Bond Lengths and Bond Angles for **3;** Table S3: The calculated and experimental geometric parameters of **2;** Table S4: The calculated and experimental geometric parameters of **3**; Table S5: The calculated and experimental chemical shifts (ppm) for **2;** Table S6: The calculated and experimental chemical shifts (ppm) for **3**.

**Author Contributions:** Conceptualization, A.B.; data curation, S.M.S., A.S.A., A.M.A.-M., M.H. and S.Y.; formal analysis, S.A., A.S.A., M.H. and S.Y.; funding acquisition, A.B.; methodology, S.A. and A.S.A.; resources, A.B.; software, S.M.S. and S.Y.; supervision, A.B.; visualization, A.M.A.-M.; writing—original draft, S.M.S. and A.B.; writing—review & editing, S.M.S. and A.B. All authors have read and agreed to the published version of the manuscript.

**Funding:** King Saud University, Saudi Arabia.

**Acknowledgments:** The authors would like to extend their sincere appreciation to the Deanship of Scientific Research at King Saud University for providing funding to this Research group NO (RGP-044).

**Conflicts of Interest:** The authors declare no conflict of interest.

## References

1. Yadav, G.; Ganguly, S. Structure activity relationship (SAR) study of benzimidazole scaffold for different biological activities: A mini-review. *Eur. J. Med. Chem.* **2015**, *97*, 419–443. [CrossRef] [PubMed]
2. Akhtar, W.; Khan, M.F.; Verma, G.; Shaquiquzzaman, M.; Rizvi, M.; Mehdi, S.H.; Akhter, M.; Alam, M.M. Therapeutic evolution of benzimidazole derivatives in the last quinquennial period. *Eur. J. Med. Chem.* **2017**, *126*, 705–753. [CrossRef] [PubMed]
3. Keri, R.S.; Hiremathad, A.; Budagumpi, S.; Nagaraja, B.M. Comprehensive Review in Current Developments of Benzimidazole-Based Medicinal Chemistry. *Chem. Biol. Drug Des.* **2014**, *86*, 19–65. [CrossRef] [PubMed]
4. Francesconi, V.; Cichero, E.; Schenone, S.; Naesens, L.; Tonelli, M. Synthesis and Biological Evaluation of Novel (thio)semicarbazone-Based Benzimidazoles as Antiviral Agents against Human Respiratory Viruses. *Molecules* **2020**, *25*, 1487. [CrossRef]
5. Singu, P.S.; Kanugala, S.; Dhawale, S.A.; Kumar, C.G.; Kumbhare, R.M. Synthesis and Pharmacological Evaluation of Some Amide Functionalized 1 H -Benzo[ d ]imidazole-2-thiol Derivatives as Antimicrobial Agents. *ChemistrySelect* **2020**, *5*, 117–123. [CrossRef]
6. Baldisserotto, A.; Demurtas, M.; Lampronti, I.; Tacchini, M.; Moi, D.; Balboni, G.; Pacifico, S.; Vertuani, S.; Manfredini, S.; Onnis, V. Synthesis and evaluation of antioxidant and antiproliferative activity of 2-arylbenzimidazoles. *Bioorg. Chem.* **2020**, *94*, 103396. [CrossRef]
7. Rahim, F.; Zaman, K.; Taha, M.; Ullah, H.; Ghufran, M.; Wadood, A.; Rehman, W.; Uddin, N.; Shah, S.A.A.; Sajid, M.; et al. Synthesis, in vitro alpha-glucosidase inhibitory potential of benzimidazole bearing bis-Schiff bases and their molecular docking study. *Bioorg. Chem.* **2020**, *94*, 103394. [CrossRef]
8. Son, D.-S.; Lee, E.-S.Y.; Adunyah, S.E. The Antitumor Potentials of Benzimidazole Anthelmintics as Repurposing Drugs. *Immune Netw.* **2020**, *20*, e29. [CrossRef]
9. Zhang, L.; Peng, X.-M.; Damu, G.L.V.; Geng, R.-X.; Zhou, C.-H. Comprehensive Review in Current Developments of Imidazole-Based Medicinal Chemistry. *Med. Res. Rev.* **2013**, *34*, 340–437. [CrossRef]
10. Boiani, M. Imidazole and Benzimidazole Derivatives as Chemotherapeutic Agents. *Mini-Rev. Med. Chem.* **2005**, *5*, 409–424. [CrossRef]
11. Refaat, H.M. Synthesis and anticancer activity of some novel 2-substituted benzimidazole derivatives. *Eur. J. Med. Chem.* **2010**, *45*, 2949–2956. [CrossRef] [PubMed]
12. Taha, M.; Mosaddik, A.; Rahim, F.; Ali, S.; Ibrahim, M.; Almandil, N.B. Synthesis, antiglycation and antioxidant potentials of benzimidazole derivatives. *J. King Saud Univ. Sci.* **2020**, *32*, 191–194. [CrossRef]
13. Vasava, M.S.; Bhoi, M.N.; Rathwa, S.K.; Jethava, D.J.; Acharya, P.T.; Patel, D.B.; Patel, H.D. Benzimidazole: A Milestone in the Field of Medicinal Chemistry. *Mini-Rev. Med. Chem.* **2020**, *20*, 532–565. [CrossRef] [PubMed]
14. Fahim, A.M.; Farag, A.; Shaaban, M.; Ragab, E. Microwave Assisted Synthesis of Pyrazolo[1, 5-a]pyrimidine, Triazolo[1,5-a]pyrimidine, Pyrimido[1,2-a]benzimdazole, Triazolo[5,1-c][1,2,4]triazine and Imidazo[2,1-c][1,2,4]triazine. *Curr. Microw. Chem.* **2019**, *5*, 111–119. [CrossRef]
15. Fahim, A.M.; Shalaby, M.A. Synthesis, biological evaluation, molecular docking and DFT calculations of novel benzenesulfonamide derivatives. *J. Mol. Struct.* **2019**, *1176*, 408–421. [CrossRef]
16. Weng, Y.; Lv, W.; Yu, J.; Ge, B.; Cheng, G. Preparation of 2,4,5-Trisubstituted Oxazoles through Iodine-mediated Aerobic Oxidative Cyclization of Enaminones. *Org. Lett.* **2018**, *20*, 1853–1856. [CrossRef]
17. Thombal, R.S.; Lee, Y.R. Synergistic Indium and Silver Dual Catalysis: A Regioselective [2 + 2 + 1]-Oxidative N-Annulation Approach for the Diverse and Polyfunctionalized N-Arylpyrazoles. *Org. Lett.* **2018**, *20*, 4681–4685. [CrossRef]
18. Apraku, J.; Okoro, C.O. Design, synthesis and anticonvulsant evaluation of fluorinated benzyl amino enaminones. *Bioorg. Med. Chem.* **2019**, *27*, 161–166. [CrossRef]
19. Baldwin, A.G.; Bevan, J.; Brough, D.; Ledder, R.G.; Freeman, S. Synthesis and antibacterial activities of enamine derivatives of dehydroacetic acid. *Med. Chem. Res.* **2017**, *27*, 884–889. [CrossRef]

20. Ali, M.; Barakat, A.; El-Faham, A.; Al-Rasheed, H.H.; Dahlous, K.; Al-Majid, A.M.; Sharma, A.; Yousuf, S.; Sanam, M.; Ul-Haq, Z.; et al. Synthesis and characterisation of thiobarbituric acid enamine derivatives, and evaluation of their α-glucosidase inhibitory and anti-glycation activity. *J. Enzym. Inhib. Med. Chem.* **2020**, *35*, 692–701. [CrossRef]
21. Mabkhot, Y.N.; Barakat, A.; Yousuf, S.; Choudhary, M.I.; Frey, W.; Ben Hadda, T.; Mubarak, M. Substituted thieno[2,3- b ]thiophenes and related congeners: Synthesis, β-glucuronidase inhibition activity, crystal structure, and POM analyses. *Bioorg. Med. Chem.* **2014**, *22*, 6715–6725. [CrossRef] [PubMed]
22. Mabkhot, Y.N.; Aldawsari, F.D.; Al-Showiman, S.S.; Barakat, A.; Soliman, S.M.; Choudhary, M.I.; Yousuf, S.; Mubarak, M.S.; Ben Hadda, T. Novel enaminone derived from thieno [2,3-b] thiene: Synthesis, x-ray crystal structure, HOMO, LUMO, NBO analyses and biological activity. *Chem. Cent. J.* **2015**, *9*, 1–11. [CrossRef]
23. Sims, G.K.; Sommers, L.E. Biodegradation of pyridine derivatives in soil suspensions. *Environ. Toxicol. Chem.* **1986**, *5*, 503–509. [CrossRef]
24. Lungu, C.; Bratanovici, B.I.; Grigore, M.M.; Antoci, V.; Mangalagiu, I.I.; Mirabela, G.M. Hybrid Imidazole-Pyridine Derivatives: An Approach to Novel Anticancer DNA Intercalators. *Curr. Med. Chem.* **2020**, *27*, 154–169. [CrossRef] [PubMed]
25. Gad, E.M.; Nafie, M.S.; Eltamany, E.H.; Hammad, M.S.A.G.; Barakat, A.; Boraei, A.T. Discovery of New Apoptosis-Inducing Agents for Breast Cancer Based on Ethyl 2-Amino-4,5,6,7-Tetra Hydrobenzo[b] Thiophene-3-Carboxylate: Synthesis, In Vitro, and In Vivo Activity Evaluation. *Molecules* **2020**, *25*, 2523. [CrossRef] [PubMed]
26. Boraei, A.T.; Sarhan, A.A.M.; Yousuf, S.; Barakat, A. Synthesis of a New Series of Nitrogen/Sulfur Heterocycles by Linking Four Rings: Indole; 1,2,4-Triazole; Pyridazine; and Quinoxaline. *Molecules* **2020**, *25*, 450. [CrossRef]
27. Boraei, A.T.; Ghabbour, H.A.; Gomaa, M.S.; El Ashry, E.S.H.; Barakat, A. Synthesis and Anti-Proliferative Assessment of Triazolo-Thiadiazepine and Triazolo-Thiadiazine Scaffolds. *Molecules* **2019**, *24*, 4471. [CrossRef]
28. Al-Majid, A.M.; Islam, M.S.; Atef, S.; El-Senduny, F.F.; Badria, F.; Elshaier, Y.A.; Ali, M.; Barakat, A.; Rahman, A.F.M.M. Synthesis of Pyridine-Dicarboxamide-Cyclohexanone Derivatives: Anticancer and α-Glucosidase Inhibitory Activities and In Silico Study. *Molecules* **2019**, *24*, 1332. [CrossRef]
29. Soliman, S.M.; Barakat, A.; Islam, M.S.; Ghabbour, H.A. Synthesis, Crystal Structure and DFT Studies of a New Dinuclear Ag(I)-Malonamide Complex. *Molecules* **2018**, *23*, 888. [CrossRef]
30. El Ashry, E.S.H.; El Kilany, Y.; Nahas, N.M.; Barakat, A.; Al-Qurashi, N.; Ghabbour, H.A.; Fun, H.-K. Synthesis and Crystal Structures of Benzimidazole-2-thione Derivatives by Alkylation Reactions. *Molecules* **2015**, *21*, 12. [CrossRef]
31. Turner, M.J.; McKinnon, J.J.; Wolff, S.K.; Grimwood, D.J.; Spackman, P.R.; Jayatilaka, D.; Spackman, M.A. Crystal Explorer17 (2017) University of Western Australia. Available online: http://hirshfeldsurface.net (accessed on 12 June 2017).
32. Frisch, M.J.; Trucks, G.W.; Schlegel, H.B.; Scuseria, G.E.; Robb, M.A.; Cheeseman, J.R.; Scalmani, G.; Barone, V.; Mennucci, B.; Petersson, G.A.; et al. *GAUSSIAN 09; Revision A02*; Gaussian Inc.: Wallingford, CT, USA, 2009.
33. Dennington, R., II; Keith, T.; Millam, J. (Eds.) *GaussView; Version 4.1*; Semichem Inc.: Shawnee Mission, KS, USA, 2007.
34. Reed, A.E.; Curtiss, L.A.; Weinhold, F. Intermolecular interactions from a natural bond orbital, donor-acceptor viewpoint. *Chem. Rev.* **1988**, *88*, 899–926. [CrossRef]
35. Marten, B.; Kim, K.; Cortis, C.; Friesner, R.A.; Murphy, R.B.; Ringnalda, M.N.; Sitkoff, D.; Honig, B. New Model for Calculation of Solvation Free Energies: Correction of Self-Consistent Reaction Field Continuum Dielectric Theory for Short-Range Hydrogen-Bonding Effects. *J. Phys. Chem.* **1996**, *100*, 11775–11788. [CrossRef]
36. Tannor, D.J.; Marten, B.; Murphy, R.; Friesner, R.A.; Sitkoff, D.; Nicholls, A.; Honig, B.; Ringnalda, M.; Iii, W.A.G. Accurate First Principles Calculation of Molecular Charge Distributions and Solvation Energies from Ab Initio Quantum Mechanics and Continuum Dielectric Theory. *J. Am. Chem. Soc.* **1994**, *116*, 11875–11882. [CrossRef]
37. Cheeseman, J.R.; Trucks, G.W.; Keith, T.A.; Frisch, M.J. A comparison of models for calculating nuclear magnetic resonance shielding tensors. *J. Chem. Phys.* **1996**, *104*, 5497–5509. [CrossRef]
38. Determann, R.; Dreher, J.; Baumann, K.; Preu, L.; Jones, P.G.; Totzke, F.; Schächtele, C.; Kubbutat, M.H.G.; Kunick, C. 2-Anilino-4-(benzimidazol-2-yl)pyrimidines—A multikinase inhibitor scaffold with antiproliferative activity toward cancer cell lines. *Eur. J. Med. Chem.* **2012**, *53*, 254–263. [CrossRef]

39. Saleh, T.S.; Al-Omar, M.A.; Abdel-Aziz, H.A. One-Pot Synthesis of Enaminones Using Golds Reagent. *Lett. Org. Chem.* **2010**, *7*, 483–486. [CrossRef]
40. Shaaban, M.R.; Saleh, T.S.; Osman, F.H.; Farag, A.M. Regioselective Synthesis of Some Novel Pyrazoles, Isoxazoles, Pyrazolo[3,4-d]pyridazines and Isoxazolo[3,4-d]pyridazines Pendant to Benzimidazole. *J. Heterocycl. Chem.* **2007**, *44*, 177. [CrossRef]
41. Stanovnik, B.; Tisler, M.; Hribar, A.; Barlin, G.; Brown, D. Methylation of heterocyclic compounds containing NH, SH and/or OH groups by means of N,N-dimethylformamide dimethyl acetal. *Aust. J. Chem.* **1981**, *34*, 1729–1738. [CrossRef]
42. Kumar, K.; Hemasunder, G.; Naidu, A.; Dubey, P.K. Alkylation studies on pyrazolyl and isoxazolyl benzimidazoles. *Heterocycl. Chem.* **2011**, *20*, 393–398.
43. Foresman, J.B.; Frisch, *Æ. Exploring Chemistry with Electronic Structure Methods*, 2nd ed.; Gaussian: Pittsburgh, PA, USA, 1996.
44. Chang, R. *Chemistry*, 7th ed.; McGraw-Hill: New York, NY, USA, 2001.
45. Kosar, B.; Albayrak, C. Spectroscopic investigations and quantum chemical computational study of (E)-4-methoxy-2-[(p-tolylimino)methyl]phenol. *Spectrochim. Acta Part A Mol. Biomol. Spectrosc.* **2011**, *78*, 160–167. [CrossRef] [PubMed]
46. Koopmans, T.A. Ordering of wave functions and eigenenergies to the individual electrons of an atom. *Physica* **1933**, *1*, 104–113. [CrossRef]
47. Parr, R.G.; Yang, W. *Density Functional Theory of Atoms and Molecules*, 1st ed.; Oxford University Press: Oxford, UK, 1989.
48. Parr, R.G.; Szentpály, L.V.; Liu, S. Electrophilicity Index. *J. Am. Chem. Soc.* **1999**, *121*, 1922–1924. [CrossRef]
49. Singh, R.; Kumar, A.; Tiwari, R.; Rawat, P.; Gupta, V. A combined experimental and quantum chemical (DFT and AIM) study on molecular structure, spectroscopic properties, NBO and multiple interaction analysis in a novel ethyl 4-[2-(carbamoyl)hydrazinylidene]-3,5-dimethyl-1H-pyrrole-2-carboxylate and its dimer. *J. Mol. Struct.* **2013**, *1035*, 427–440. [CrossRef]